REMARKS/ARGUMENTS

Claims 4, 6, 7, and 15 are pending in this application. By this Amendment, Applicant cancels Claim 1 and amends Claims 4, 6, 7, and 15.

Claims 1 and 15 were rejected under 35 U.S.C. § 102(e) as being anticipated by or, in the alternative under 35 U.S.C. § 103(a) as obvious over Kadota et al. (U.S. 6,946,930). Claims 1 and 15 were rejected under 35 U.S.C. § 103(a) as being unpatentable over Kadota et al. in view of Campbell et al. (U.S. 6,462,698). Claim 4 was rejected under 35 U.S.C. § 103(a) as being unpatentable over Kadota et al. in view of Yoneda et al. (U.S. 6,271,617). Claim 4 was rejected under 35 U.S.C. § 103(a) as being unpatentable over Kadota et al. and Campbell et al. in view of Yoneda et al. Claim 6 was rejected under 35 U.S.C. § 103(a) as being unpatentable over Kadota et al. in view of Oshio (U.S. 2004/0164645). Claim 6 was rejected under 35 U.S.C. § 103(a) as being unpatentable over Kadota et al. and Campbell et al., and further in view of Oshio. Claim 7 was rejected under 35 U.S.C. § 103(a) as being unpatentable over Kadota et al. in view of Sato et al. (U.S. 4,340,834). Claim 7 was rejected under 35 U.S.C. § 103(a) as being unpatentable over Kadota et al. and Campbell et al. in view of Sato et al. Claim 1 has been canceled, and Claim 6 has been amended to be in independent form including all of the features of Claim 1. Applicant respectfully traverses the rejections of Claims 4, 6, 7, and 15.

Claim 6 has been amended to recite:

> A surface acoustic wave filter comprising:
> a piezoelectric substrate; and
> an input-side IDT electrode and an output-side IDT electrode arranged on the piezoelectric substrate so as to be separated from each other in the propagation direction of a surface acoustic wave; wherein
> the piezoelectric substrate is a crystal substrate;
> the input-side IDT electrode and the output-side IDT electrode each include an electrode layer made of Al or an Al alloy defining a major electrode layer, and the electrode film thickness ratio h/λ is in the range of from about 0.035 to about 0.06, wherein h represents the film-thickness of the input-side IDT electrode and the output-side IDT electrode, and λ represents the wavelength of the surface acoustic wave;

at least one of the input-side IDT electrode and the output-side IDT electrode is an SPUDT electrode; and

the crystal substrate is an ST-cut crystal substrate having an Euler's angle (0, θ, 0), and the angle θ is in the range represented by θ = {−3·(h/λ)×100+134}±1. (emphasis added)

The Examiner alleged that Kadota et al. and the combination of Kadota et al. and Campbell et al. teach all of the features recited in Applicant's Claim 6, except for the Euler angles of the substrate. The Examiner further alleged that Oshio teaches a substrate having the Euler angles recited in Applicant's Claim 6. Thus, the Examiner concluded that it would have been obvious to use the design of Kadota et al. and the design of the combination of Kadota et al. and Campbell et al. "with the Euler angles of Oshio since with such angles 'it is possible to lower the loss accompanied with the propagation ... thereby improving the Q value', as Oshio notes in paragraph 17." Applicant respectfully disagrees.

Section 2.1 on page 100 of the attached Fujitsu Scientific & Technical Journal, December 1981 specifically discloses that the propagation direction of SH waves on a ST-cut quartz **is perpendicular to** the propagation direction of Rayleigh waves on the ST-cut quartz.

Kadota et al. teaches a surface acoustic wave device which utilizes an SH wave on an ST-cut 90° X-propagation quartz substrate with Euler angles (0°, θ, 90°±2°). If, as alleged by the Examiner, the substrate of Oshio having Euler angles (0°, 100 to 150°, 0°) were substituted for the substrate of Kadota et al., then the surface acoustic wave device of Kadota et al. would inherently utilize a Rayleigh wave instead of an SH wave since the propagation direction (0°) of the substrate of Oshio would be perpendicular to the propagation direction (90°±2°) of the substrate of Kadota et al. In other words, the Examiner's proposed modification to Kadota et al. would render the surface acoustic wave device of Kadota et al. unsatisfactory for it's intended purpose, i.e., to propagate SH waves.

The Examiner is reminded that if the proposed modification would render the prior art invention being modified unsatisfactory for its intended purpose, then there is

no suggestion or motivation to make the proposed modification. In re Gordon, 733 F.2d 900, 221 USPQ 1125 (Fed. Cir. 1984) and MPEP § 2143.01.

Accordingly, Applicant respectfully requests reconsideration and withdrawal of the rejection of Claim 6 under 35 U.S.C. § 103(a) as being unpatentable over Kadota et al. in view of Oshio, and the rejection of Claim 6 under 35 U.S.C. § 103(a) as being unpatentable over Kadota et al. and Campbell et al., and further in view of Oshio.

The Examiner relied upon Yoneda et al. and Sato et al. to allegedly cure various deficiencies of Kadota et al. and Campbell et al. However, neither Yoneda et al. nor Sato et al. teaches or suggests the feature of "the crystal substrate is an ST-cut crystal substrate having an Euler's angle (0, θ, 0), and the angle θ is in the range represented by $\theta = \{-3\cdot(h/\lambda)\times 100+134\}\pm 1$" as recited in Claim 6. Thus, Applicant respectfully submits that Yoneda et al. and Sato et al. fail to cure the deficiencies of Kadota et al. and Campbell et al.

Accordingly, Applicant respectfully submits that Kadota et al., Campbell et al., Oshio, Yoneda et al., and Sato et al., applied alone or in combination, fail to teach or suggest the unique combination and arrangement of elements recited in Applicant's Claim 6.

In view of the foregoing amendments and remarks, Applicant respectfully submits that Claim 6 is allowable. Claims 4, 7, and 15 depend upon Claim 6, and are therefore allowable for at least the reasons that Claim 6 is allowable.

In view of the foregoing amendments and remarks, Applicant respectfully submits that this application is in condition for allowance. Favorable consideration and prompt allowance are solicited.

To the extent necessary, Applicant petitions the Commissioner for a Two-Month Extension of Time, extending to October 25, 2006, the period for response to the Office Action dated May 25, 2006.

The Commissioner is authorized to charge any shortage in fees due in connection with the filing of this paper, including extension of time fees, to Deposit Account No. 50-1353.

Respectfully submitted,

Dated: October 19, 2006

/Christopher A. Bennett #46,710/
Attorneys for Applicant(s)

KEATING & BENNETT, LLP
8180 Greensboro Drive, Suite 850
Tyson's Corner, VA 22102
Telephone: (703) 637-1480
Facsimile: (703) 637-1499

Joseph R. Keating
Registration No. 37,368

Christopher A. Bennett
Registration No. 46,710

JN S0036A (FUSTA) (0016-2523) Fujitsu Sci Tech J.
VN VOL. 17, NO. 4 PAGE. 99-113 1981
CI (A) (41) (EN) (JPN) (写図13, 表1, 参10)
AB SH型，すなわち水平偏波せん断波型の表面弾性波（SAW）に関する理論的，実験的研究を述べた。基板の表面近くを伝搬する表面層バルク波は位相速度が高いので，高周波応用に適すると考えられる。しかしながら，これらの波はバルク波であり，基板の表面が自由である時にのみ存在し，進行中に振幅が減衰する。これらの波について，インタディジタル電極の機械負荷効果を考慮して解析した。計算結果，実験結果によれば，電気機械結合係数，変位分布などの弾性特性は電極の厚みに大きく依存し，そのため，SH型SAWとして取扱うべきであることが分かった
CC [illegible] (534-16:539.2, 621.382:534.2)
KW 弾性表面波素子; 電極; くし形; 石英; 弾性波; 基板; 実体波; Rayleigh

2

SH-Ty[illegible] on Rotated Y-Cut Quartz

By Tsutomu Nishikawa, Atsushi Tani and Chikao Takeuchi

(Manuscript received June 12, 1981)

This paper describes theoretical and experimental studies of SH-type or horizontally polarized shear wave type surface acoustic waves on rotated Y-cut quartz.

Surface skimming bulk waves propagating near the surface of a substrate are considered suitable for high frequency applications because of their high phase velocity. However, these waves are bulk waves, and they exist only when the surface of a substrate is free. Moreover, their amplitudes decay as they travel.

These waves have been analyzed with the mechanical loading effect of interdigital electrodes taken in account. The calculated and experimental results indicate that acoustic properties, such as electromechanical coupling coefficients and displacement distributions, are largely dependent on the thickness of the electrodes, and that these waves should be treated as SH-type surface acoustic waves or Love waves. In addition, the results indicate that devices with lower insertion losses can be obtained if the thickness of the electrodes is increased.

1. Introduction

Rayleigh waves on ST-cut quartz are commonly used for surface acoustic wave (SAW) devices because of their good temperature characteristics. However,

their comparatively low phase velocity (3160 m/s) makes it difficult to obtain high frequency SAW devices. Also, bulk wave modes, such as the shear wave mode and longitudinal wave mode, are generated and cause spurious responses.

Recently, bulk waves propagating near the surface of a substrate {called surface skimming bulk waves (SSBW) or shallow bulk acoustic waves (SBAW)} have been reported[1)-4)]. These bulk waves have many advantages over the conventional Rayleigh waves, such as higher phase velocity, good temperature stability and fewer spurious responses, and are considered practical for higher frequency devices. Some analytical methods for SSBW have been reported[1),4)]. In these methods, however, the mechanical loading effect of interdigital electrodes is ignored and the surface of a substrate is assumed to be free. In the interdigital transducer (IDT) regions this effect cannot be ignored.

This paper describes a method for analysing these waves which takes into account the mechanical loading effect of the interdigital electrodes[5)-7)]; it also describes the calculated and experimental parameters of these waves, such as phase velocity, temperature coefficients, electromechanical coupling coefficients and displacement distributions. In addition, some experimental results of a 1.6 GHz SAW filter using conventional photolithographic techniques are presented.

2. Analysis of SH-type surface acoustic waves

2.1 Analytical method

Figure 1 shows the rotated Y-cut quartz. θ is the rotation angle and Z' (the x_3 axis) is the direction of wave propagation. This propagation direction is perpendicular to that of Rayleigh waves on ST-cut quartz. Since it is difficult to obtain exact solutions which include the effect of wave reflection at the interdigital electrodes, we have assumed that the entire surface is overlaid with a thickness of metal as shown in Fig. 2[8)].

Assuming uniformity of displacements (u_i; $i = 1, 2, 3$) and electric potential (φ) in the x_1 direction, we consider the wave propagation in the x_3 direction. Let the displacements and electric potential be

$$u_i = A_i \exp\{ j(\omega t + \eta x_2 - \xi x_3) \}, \; i = 1, 2, 3, \qquad \cdots\cdots\cdots (1)$$

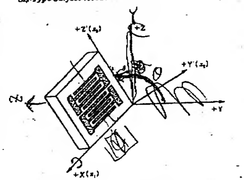

Fig. 1—Coordinate system on rotated Y-cut quartz.

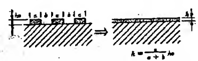

Fig. 2—Approximated interdigital transducer model.

and

$$\varphi = A_4 \exp\{j(\omega t + \eta x_2 - \zeta x_3)\}, \quad \cdots\cdots (2)$$

where η and ζ are wave propagation constants in the x_2 and x_3 directions, respectively. The stress equation of motion and charge equation of electrostatics are shown below:

$$T_{ij,i} = \rho \ddot{u}_j, \quad \cdots\cdots (3)$$

and

$$D_{i,i} = 0. \quad \cdots\cdots (4)$$

Substituting equations (1) and (2) into (3) and (4), we obtain the following

frequency equation on rotated Y-cut quartz.

$$\begin{pmatrix} a_{11} & a_{12} & 0 & 0 \\ a_{21} & a_{22} & 0 & 0 \\ 0 & 0 & a_{33} & a_{34} \\ 0 & 0 & a_{43} & a_{44} \end{pmatrix} \begin{pmatrix} A_1 \\ A_4 \\ A_2 \\ A_3 \end{pmatrix} = 0, \quad \cdots\cdots (5)$$

where,

$$a_{11} = c_{66}K^2 - 2c_{56}K + c_{55} - \bar{c}_{66}X^2,$$
$$a_{12} = e_{26}K^2 - (e_{25} + e_{36})K + e_{35},$$
$$a_{22} = -(\epsilon_{22}K^2 - 2\epsilon_{23}K + \epsilon_{33}),$$
$$a_{33} = c_{22}K^2 - 2c_{24}K + c_{44} - \bar{c}_{66}X^2,$$
$$a_{34} = c_{24}K^2 - (c_{44} + c_{23})K + c_{34},$$
$$a_{44} = c_{44}K^2 - 2c_{34}K + c_{33} - \bar{c}_{66}X^2,$$
$$a_{ij} = a_{ji},\ K = \eta/\zeta,\ \bar{c}_{66} = c_{66} + e_{26}^2/\epsilon_{22},\ X = V_s/V_b, \text{ and } V_b = \sqrt{\bar{c}_{66}/\rho}.$$

V_s is the SAW phase velocity, and c_{ijkl}, e_{kij} and ϵ_{ij} are the elastic, piezoelectric and dielectric constants, respectively. As shown in equation (5), the frequency equation is very simple compared with that for Rayleigh waves on rotated Y-cut quartz. Only displacement u_1 is coupled to electric potential. This indicates that u_1 and φ should be analyzed as SH-type SAW. Moreover, the fact that u_2 and u_3 cannot be generated by piezoelectricity implies that no spurious response occurs. General solutions for u_1 and φ can be obtained by solving the following fourth order equation in terms of K for a given X,

$$\begin{vmatrix} c_{66}K^2 - 2c_{56}K + c_{55} - \bar{c}_{66}X^2 & e_{26}K^2 - (e_{25} + e_{36})K + e_{35} \\ e_{26}K^2 - (e_{25} + e_{36})K + e_{35} & -(\epsilon_{22}K^2 - 2\epsilon_{23}K + \epsilon_{33}) \end{vmatrix} = 0, \cdots (6)$$

and selecting two roots which satisfy the boundary conditions where x_2 approaches infinity. The solutions are given by:

$$u_1 = \sum_{n=1}^{3} C(n) A_1^{(n)} \exp[j\{K(n)\xi x_2 - \xi x_3 + \omega t\}], \quad \cdots\cdots (7)$$

and

$$\varphi = \sum_{n=1}^{3} C(n) A_4^{(n)} \exp[j\{K(n)\xi x_2 - \xi x_3 + \omega t\}]. \quad \cdots\cdots (8)$$

On the other hand, the solution for displacement (u_1') in the metal layer is obtained from the stress equation of motion, and is given by the following expression.

$$u_1' = \sum_{n=2}^{4} C(n) \exp[j\{K(n)\xi x_2 - \xi x_3 + \omega t\}], \quad \cdots\cdots\cdots (9)$$

where $K(3) = -K(4) = \sqrt{(V_e/V_s)^2 - 1}$, $V_e = \sqrt{\mu/\rho'}$, and μ and ρ' are the Lamé constant and the density of the metal.

The boundary conditions between the substrate and the layer are shown as follows:

$$u_1 = u_1' \quad \text{at } x_2 = 0, \quad \cdots\cdots\cdots\cdots\cdots\cdots (10)$$

$$T_{12} = T_{12}' \text{ at } x_2 = 0, \quad \cdots\cdots\cdots\cdots\cdots\cdots (11)$$

$$\varphi = 0 \quad \text{at } x_2 = 0, \quad \cdots\cdots\cdots\cdots\cdots\cdots (12)$$

and

$$T_{12}' = 0 \quad \text{at } x_2 = h. \quad \cdots\cdots\cdots\cdots\cdots\cdots (13)$$

Substituting general solutions (7), (8) and (9) into the above boundary conditions, we obtain the following homogeneous equation.

$$\begin{pmatrix} S(1) & S(2) & -\mu K(3) & -\mu K(4) \\ A_1^{(1)} & A_1^{(2)} & -1 & -1 \\ 0 & 0 & S(3) & S(4) \\ A_4^{(1)} & A_4^{(2)} & 0 & 0 \end{pmatrix} \cdot \begin{pmatrix} C(1) \\ C(2) \\ C(3) \\ C(4) \end{pmatrix} = 0, \quad \cdots (14)$$

where

$$S(1) = \{c_{66}K(1) + c_{14}\} A_1^{(1)} + \{e_{26}K(1) + e_{36}\} A_4^{(1)},$$

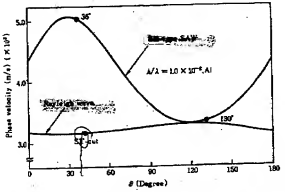

Fig. 3–Phase velocities of SH-type SAW and Rayleigh waves on rotated Y-cut quartz.

$$S(2) = \{c_{66}K(2) + c_{14}\} A_1^{(2)} + \{e_{26}K(2) + e_{36}\} A_4^{(2)},$$

$$S(3) = \mu K(3) \exp\{j\xi K(3)h\},$$

and

$$S(4) = \mu K(4) \exp\{j\xi K(4)h\}.$$

The phase velocity is obtained when the determinant of equation (14) is zero.

2.2 Calculated results

The calculated phase velocity of SH-type SAW on rotated Y-cut quartz is shown in Fig. 3. The curve is calculated with an aluminum (Al) layer thickness of 0.01λ (λ: wavelength). The phase velocity of Rayleigh waves is also shown in the figure. It can be seen that the phase velocity on 36° rotated Y-cut quartz is 1.6 times that of Rayleigh waves on ST-cut quartz.

Figure 4 shows the first and second order frequency temperature coefficients. Seven frequency points are calculated at 10 °C intervals from −5 °C to +55 °C and coefficients are obtained using the method of least squares. It can

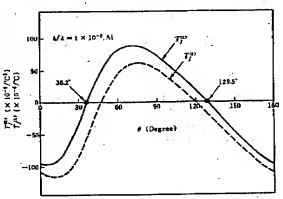

Fig. 4—First and second order frequency temperature coefficients.

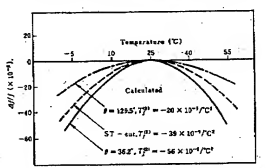

Fig. 5—Calculated frequency temperature characteristics.

be found that the rotation angles where the first order temperature coefficient is zero are 36.2° and 129.5°. The frequency temperature characteristics of these rotation angles are shown in Fig. 5, where they are compared with that of Rayleigh waves on ST-cut quarts.

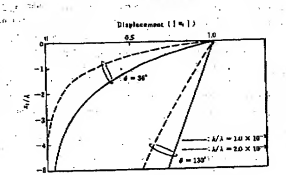

Fig. 6—Displacement distributions for depth on 36° and 130° rotated Y-cut quarts when the surface is overlaid with aluminum.

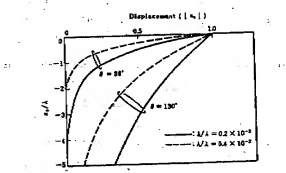

Fig. 7—Displacement distributions for depth when gold is used instead of aluminum.

Figure 6 shows the displacement distributions for depth on 36° and 130° rotated Y-cut quarts when the surface is overlaid with a thin aluminum layer. As the thickness of the layer increases, the displacements concentrate more to the surface. Also, the effect of the Al layer thickness at 36° is larger than that

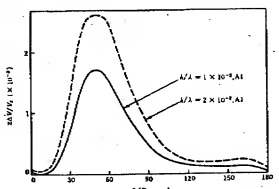

Fig. 8—Electromechanical coupling coefficients of SH-type SAW on rotated Y-cut quarts.

at 130°. This is because the phase velocity at 36° (5088 m/s) is very high compared with that of the Al shear wave (3100 m/s), while in the case of 130° rotation the phase velocity (3330 m/s) approximates that of the Al shear wave, resulting in minimal effect on the displacement. In high frequency operation, SH-type SAW devices can be easily obtained on 36° rotated Y-cut quarts using thin Al electrodes. Figure 7 shows the displacement distributions when gold (Au) is used instead of aluminum. The mechanical loading effect of a gold layer is very large compared with that of Al, because gold's shear wave velocity (1250 m/s) is very low and its density is very high. The figure shows that the displacements concentrate more to the surface even though the Au layer is very thin.

Since the displacement distribution depends largely on the thickness of the layer, the effective electromechanical coupling coefficients should also change. The coupling coefficients, $2\Delta V/V_0$, are calculated from the difference in phase velocities obtained from electrical boundary conditions (12) and (15)

$$D_2 = 0 \quad \text{at} \quad x_2 = 0 \,. \qquad \cdots\cdots\cdots\cdots\cdots\cdots\cdots\cdots \quad (15)$$

The coupling coefficients with an Al layer thickness of 0.01λ and 0.02λ are

Table 1. Design parameters of experimental samples

	Type-1	Type-2
Substrate Rotation angle (θ)	36°	36°
Transducer Configuration		
Finger pairs	80-160-80	150-150
Wavelength (λ)	11.9 μm	3.18 μm
Finger width	$\lambda/8$	$\lambda/4$
Path length (d)	$\lambda/4$	7λ

shown in Fig. 8. The coupling coefficients are heavily dependent on the thickness of the layer.

3. Experimental results

Table 1 outlines the samples used in the experiments. A substrate of 36° rotated Y-cut quarts was used because of its high phase velocity and good temperature characteristics.

In Type-1, the double electrode transducer was used for comparison with the calculated results. The path length between input- and output-transducer was designed to be very short ($\lambda/4$) to avoid increased propagation loss on the free surface. The attenuation characteristics of the Type-1 transducer with electrode thicknesses of 100 nm and 200 nm are shown in Fig. 9. The center frequency and insertion loss depend largely on the thickness of the electrodes. These results indicate that the mechanical loading effect of interdigital electrodes simply can not be ignored.

The phase velocity and coupling coefficient were obtained from the characteristics shown in Fig. 9. The phase velocity was calculated from the center fre-

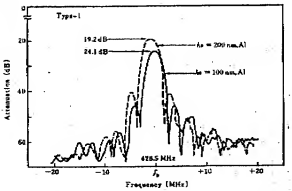

Fig. 9—Attenuation characteristics of the Type-1 transducer for electrode thicknesses of 100 nm and 200 nm.

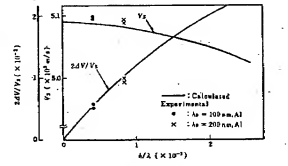

Fig. 10—Phase velocity and electromechanical coupling coefficient variation with different electrode thicknesses on 36 ° rotated Y-cut quartz.

quency of the filter and the coupling coefficient was obtained from the minimum insertion loss at the center frequency using an IDT cross field model[9),10)]. Experimental and calculated results are shown in Fig. 10, and can be seen to

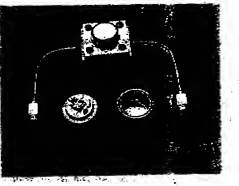

Fig. 11—The 1.6 GHz SH-type SAW filter.

agree closely. These results indicate that the approximated model assumed previously is viable, and that these waves can be treated as SH-type SAW if the propagation path is very short or overlaid with metal film.

Another type of the transducer, Type-2, was used to demonstrate the applicability of SH-Type SAW filters at frequencies above 1 GHz using conventional photolithographic techniques. In order to achieve high loaded Q and low insertion loss, a resonator-type SAW filter was designed which uses wave reflection at the finger edges of the interdigital electrodes. The thickness of the electrodes was 40 nm. A photograph of the sample is shown in Fig. 11.

Figures 12-a) and -b) show attenuation characteristics of this filter. The center frequency was 1.6 GHz, and high loaded Q (1000) and low insertion loss (9.8 dB) were obtained. The relative attenuation from 0 GHz to 3.2 GHz was more than 38 dB, and no spurious response was caused by bulk waves. Figure 13 shows the frequency temperature characteristics. The turnover temperature difference between the calculated and experimental values was less than 5 °C, and the second order temperature coefficient, calculated as $-56 \times 10^{-9}/°C^2$, was found to be $-50 \times 10^{-9}/°C^2$.

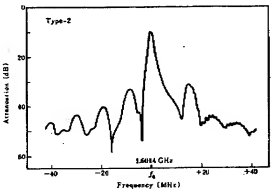

a) Narrowband attenuation characteristics.

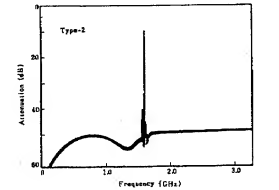

b) Wideband attenuation characteristics.

Fig. 12—Attenuation characteristics of 1.6 GHz SH-type SAW filter.

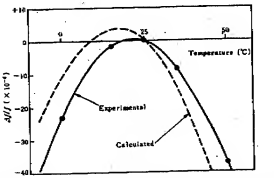

Fig. 13—Frequency temperature characteristics of 1.6 GHz SH-type SAW filter.

4. Conclusion

SH-type surface acoustic waves on rotated Y-cut quartz have been analyzed assuming that SSBW would change to SH-type SAW if the surface of the substrate were overlaid with metal film. The calculated and experimental results are in close agreement. The results indicate that this assumption is valid even in IDT regions if the propagation path is very short or if it is overlaid with film. Also, the experimental results for the 1.6 GHz SAW filter indicate that this type of wave, especially on 36 ° rotated Y-cut quartz, is very practical for several GHz SAW devices because of its high phase velocity and good temperature stability.

5. Acknowledgement

The authors would like to thank Messrs. M. Otsuki, T. Kojima and K. Shitsi for their constant guidance and encouragement.